Enhancement of NH_3 gas sensing with Ag-Pt co-catalyst on SnO_2 nanofilm for medical diagnosis

Duong Thi Thuy Trang[1], Nguyen Van Duy[1,*], Dang Thi Thanh Le[1], Chu Manh Hung[1], Matteo Tonezzer[2,3], Hugo Nguyen[4], Nguyen Duc Hoa[1]

[1]ITIMS, Hanoi University of Science and Technology (HUST), Hanoi, Vietnam

[2]Center Agriculture Food Environment, University of Trento/Fondazione Edmund Mach, Via E. Mach 1, 38010 San Michele all'Adige, Italy

[3]IMEM-CNR, Sede di Trento—FBK, Via alla Cascata 56/C, Povo, 38123 Trento, Italy

[4]Uppsala University, Department of Engineering Sciences, Lägerhyddsvägen 1, 751 21 Uppsala, Sweden

Corresponding author email: nguyenvanduy@itims.edu.vn.

Abstract.

Nanoparticles of noble metals are known to have a catalytic effect on the performance of SnO_2 nanomaterial as a gas sensing material. In this work, Ag, Pt and Ag-Pt bimetallic nanoparticles were used to decorate thin films of SnO_2 making different gas sensors. Both Ag and Pt alone improved the sensor performance, but the bimetal alloy improved the sensor performance much more. The right ratio of the bimetal made the sensor very sensitive to NH_3, so that it was able to quickly (12 s) detect 1 part per million of NH_3 with a response of 4.31 at a temperature of 250 °C. The sensor limit of detection for NH_3 was less than 10 parts per billion. The response of the sensor was negligibly affected by humidity and interfering gases. The results showed that the tiny and inexpensive sensor developed in this work can be used in breath analysis for early diagnosis.

Keywords: ammonia, gas sensor, SnO_2 nanofilm, Ag-Pt nanoalloy, breath diagnosis.

Introduction

In recent years, the development of small, simple and inexpensive sensors for detecting specific gases for different applications has attracted a lot of attention from materials scientists. Ammonia (NH_3) is a harmful gas present in the atmosphere and increasingly emitted by human activities [1]. The human nose can detect NH_3 at a concentration of 30–50 parts per million (ppm) [2], but it is already harmful below this threshold [3].

In addition to industrial processes, NH_3 is also produced in the human and animal body by the metabolism of amino acids and proteins [4]. In normal conditions, NH_3 is absorbed and metabolized in the liver to a waste product called urea and excreted in the urine. If the body is unable to process NH_3 and reduce its amount, it will build up in the blood and reach a level that can lead to serious health problems, including brain damage, coma and even death. The detection of NH_3 in the breath agrees well with the *blood urea nitrogen* (BUN) medical test, which is the reference technique for this type of measurement. A gas sensor can therefore be used to monitor the level of NH_3 in the blood as long as it is capable of detecting concentrations around one part per million (ppm) [5]. The breath test is quick, non-invasive and simple to use compared to blood tests which are time consuming and labor intensive, and therefore can also be used to evaluate liver function and NH_3 cycle problems, as well as infections such as those caused by common and dangerous *Helicobacter pylori* [6].

Tin oxide is one of the most widely used metal oxides in resistive gas sensors, but unfortunately its sensitivity is not sufficient to detect the low concentrations required for breath analysis. Yi et al. reported on pure SnO_2 that had a response from 1.25 (at 200 °C) to 1.32 (at 350 °C) towards 100 ppm of NH_3 [7]. Guo et al. calculated a response of 1.45 for mesoporous SnO_2 tested at 260 °C towards 100 ppm of NH_3 [8]. These response values are quite low and need to be improved for practical application. In recent years, the improvement has been made, for example, by means of surface decoration with metal nanoparticles (Ag, Au, Pd, Pt...) which promotes the spill-over and the Fermi-level control [9–14]. Among these metal catalysts, Pt is

one of the most used, as it greatly improves the response of the MOS sensors. For example, Wang and his group showed that the surface decoration of SnO_2 with platinum increases the response from 1.2 to 24.0 towards 200 ppm of NH_3 at 160 °C [15]. Shahabuddin et al. confirmed that Pt increased the SnO_2 response from 1.60 (at 250 °C) to 25.7 (at 230 °C) towards 450 ppm of NH_3 [16]. Silver has also been shown to have a positive influence on the sensing performance of MOS sensors [17]. Hwang and coworkers found that SnO_2 decorated with Ag nanoparticles working at 450 °C showed a 3.7-fold improvement over pure SnO_2 in response to 100 ppm ethanol [18]. Recently, the properties of Ag-Pt alloy nanoparticles have also attracted a lot of attention from many researchers. It has been shown to have greater effect than the individual metals in electrocatalysis, photocatalysis (degradation of methyl orange) and low-temperature oxidation of methanol [17,19–21]. To our knowledge, decoration with Pt-Ag alloy nanoparticles has not yet been studied in the field of gas sensors. In this work, sputtering is used to fabricate resistive gas sensors based on pure SnO_2, Pt/SnO_2, Ag/SnO_2 and $Pt\text{-}Ag/SnO_2$, and their performance in detecting low concentrations of NH_3 for biomedical applications are studied.

Experimental

The deposition and patterning of the electrodes and the sensing material are described step by step in Fig. 1. Two metal electrodes and a microheater, composed of two layers of Cr/Pt (5/100 nm) were deposited by UV lithography, sputtering and lift-off on SiO_2/Si substrates. The sensing materials (pure SnO_2, Ag/SnO_2, Pt/SnO_2 and $Pt\text{-}Ag/SnO_2$) were then deposited in the form of thin films that connect the two electrodes on each sensor. The parameters for SnO_2 sputtering were $5x10^{-3}$ mTor, 30 W and 20/10 sccm of Ar/O_2 flow rate, while for electrodes and metal catalysts sputtering they were 10 W and an Ar flow of 30 sccm.

The thickness of the SnO_2 film was around 50 nm in all samples, while the thicknesses of the Ag and Pt layers were varied to investigate their influence on the sensor performance. The

different thicknesses of the Ag and Pt layers were controlled by the sputtering time: 20, 40 and 80 seconds to obtain Ag layers of 1, 2 and 4 nm, respectively, and 30, 60 and 120 s to obtain Pt layers of 1, 2 and 4 nm, respectively. It should be noted that sputtering of a few nm did not produce a continuous layer of material, but for simplicity in this work the layer thickness will be used to name the samples: depending on the nominal thickness of the sensing material layers, the samples were named as SnO_2, P1, P2, P4, A1, A1P1, A1P2, A1P4, A2P2 and A4P2 (see Table 1).

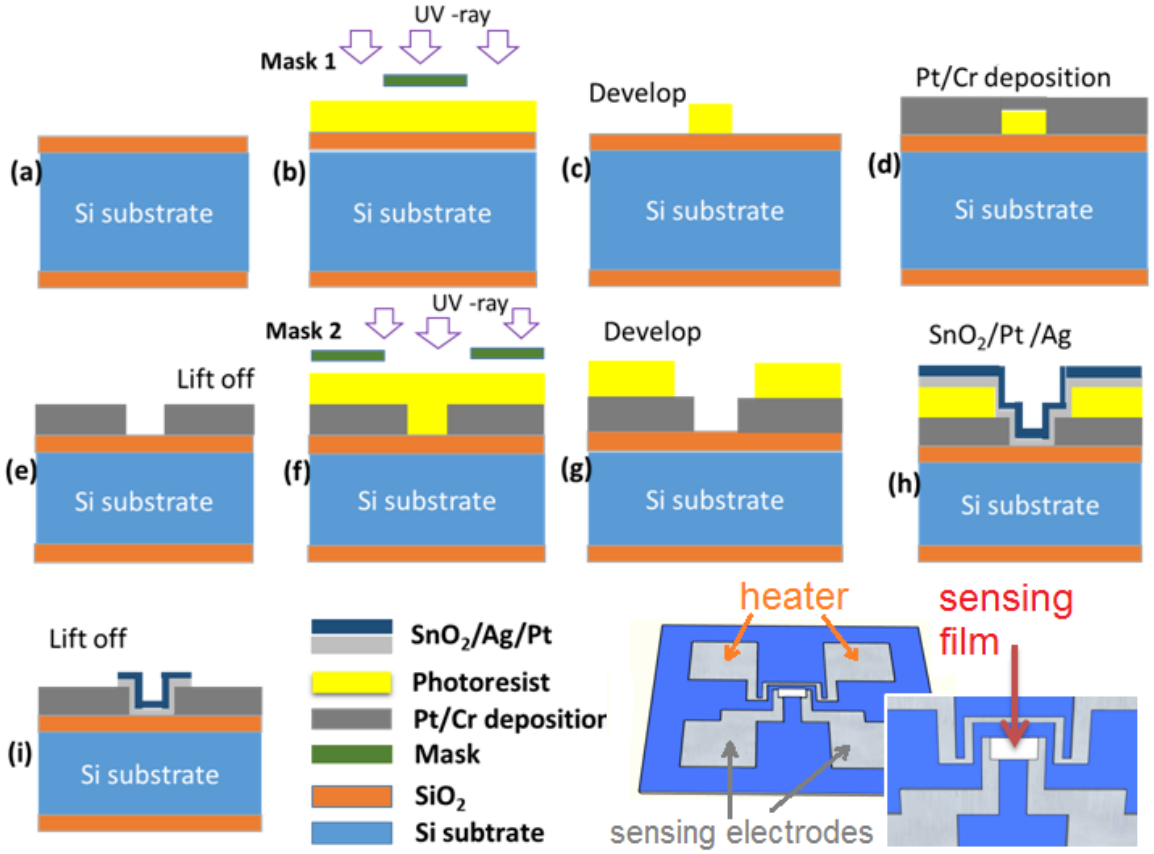

Figure 1. Scheme of the sensor fabrication steps.

Table 1. Prepared sensor samples, the name of which reflects the materials used and their thickness.

No.	Material	Sputtering time (s)	Thickness (nm)	Sample name
1	SnO_2	420	50	SnO_2
2	Pt	30	1	P1
3	Pt	60	2	P2
4	Pt	120	4	P4

5	Ag	20	1	A1
6	Ag/Pt	20/30	1/1	A1P1
7	Ag/Pt	20/60	1/2	A1P2
8	Ag/Pt	20/120	1/4	A1P4
9	Ag/Pt	40/60	2/2	A2P2
10	Ag/Pt	80/60	4/2	A4P2

All samples were heat treated at 500 °C in ambient air for 3 hours in order to stabilize the nanomaterial and improve its sensing performance. Morphology, structure and composition of the thin films were investigated using scanning electron microscopy (SEM), X-ray diffraction (XRD), energy dispersion spectroscopy (EDS) and X-ray photoelectron spectroscopy (XPS).

The sensors were characterized in a home-built system comprising a measurement chamber with a hot plate as sensor holder, microprobes and gas flow controllers connected to high purity gas bottles. The sensors signal was acquired through a Keithley 2450 Sourcemeter and processed with a home-built data acquisition system developed in LabView (National Instruments) environment. The devices were initially measured at different temperatures of 200, 250, 300 and 350 °C, with selected concentrations of 250, 100, 50 and 25 ppm of NH_3. The sensor response was defined as $S = R_{air}/R_{gas}$, where R_{air} and R_{gas} were respectively the resistance of the sensor in presence of air and target gas. Response time and recovery time were calculated as the time it took for the sensor to reach 90% of the maximum response and to drop to 90% of full recovery, respectively. The limit of detection was calculated as $3\frac{noise_{rms}}{slope}$, where $noise_{rms}$ was the standard deviation of the sensor signal and *slope* was the derivative of the sensor response as a function of the NH_3 concentration.

Results and discussion

SEM images of three thin films used as sensing materials are shown in Fig. 2. Figure 2(A) and (B) show the pure SnO_2 film, respectively from the top and from the side. The film is uniform with small grains (16-34 nm) without cracks and with a thickness of about 50 nm. Figures 2(C)

and (D) show the samples P2 and A1P2, respectively. Here, the sensing materials tend to cluster into larger particles (35-55 nm) than in the pure SnO_2 sample, but the films are still uniform.

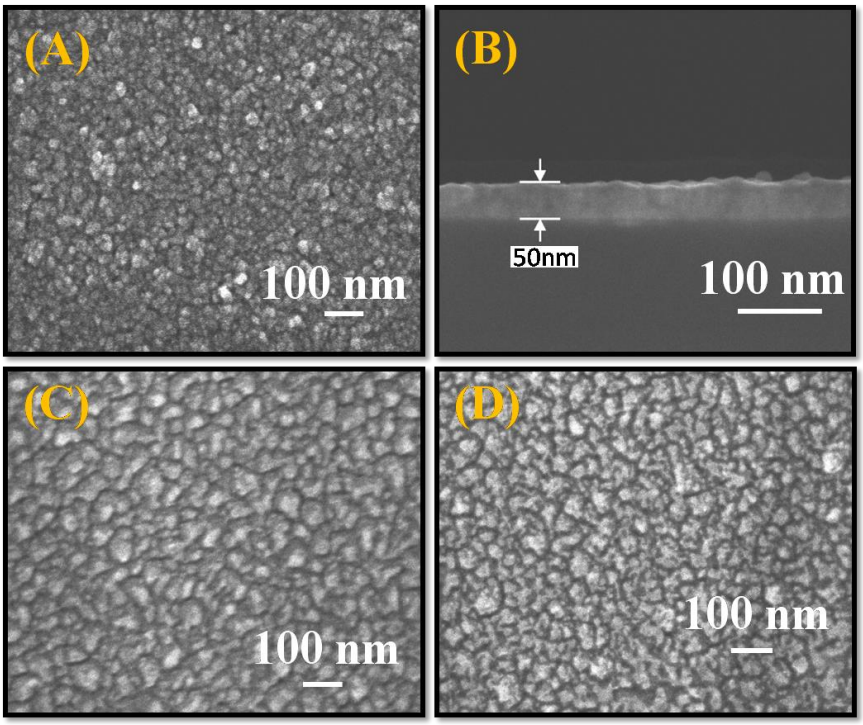

Figure 2. SEM images of thin films of sensing materials. A) and B) pure SnO_2 (top view and cross section); C) P2 sample, D) A1P2 samples (both top view).

The crystal structures of the films studied by XRD are shown in Fig. 3(A). As the film thickness was just 50 nm, the intensity of all diffraction peaks was quite weak. The black pattern at the bottom comes from the pure SnO_2 film, showing four peaks at angles of 26.6°, 33.9°, 37.9° and 51.8°, corresponding to planes (110), (101), (200) and (211) of the rutile structure of SnO_2, respectively. This result is consistent with the JCPDS card 41-1445 of SnO_2 [22]. Going up, the other patterns correspond to samples A1 (in red), P2 (in green) and A1P2 (in blue). In pattern A1, two additional peaks at 38.1° and 44.3° are present, indexed by a yellow triangle as planes (111) and (200) from Ag nanoparticles according to JCPDS card 04-0783 [23]. The position of the peak relative to the Pt nanoparticles is indicated by a red star in the pattern of P2 sample at 40.0°, corresponding to the plane (111) of Pt (JCPDS card 65-2868). For the A1P2 sample pattern, the intensity of the Ag and Pt peaks is significantly reduced, and this may indicate a

conversion of Ag and Pt to another structure. In all patterns, the strongest peak at 33.0° comes from the Si substrate. Using the Scherrer equation to estimate the crystallite size of the SnO_2 nanostructured thin film, we obtained values of approximately 5.6 nm. The EDS spectrum of the thin film A1P2 in Fig. 3 (B) shows that the elements Sn, O, Ag and Pt are present as expected, while there are no other elements indicating impurities. The EDS spectrum indicates that both Ag and Pt are present in very small amounts, of 1.7 and 0.9%, respectively.

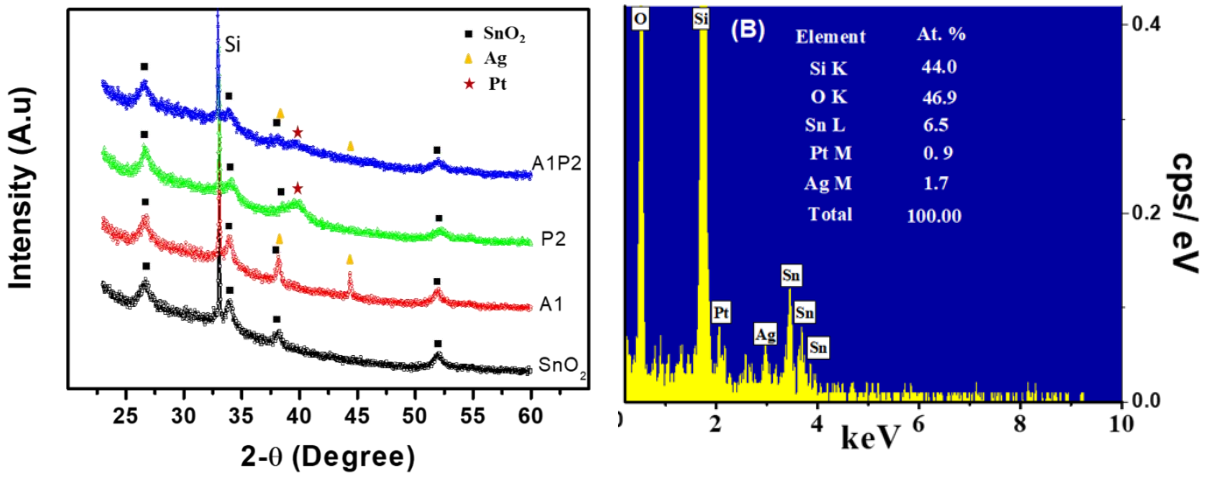

Figure 3. (A) XRD patterns of the SnO_2, A1, P2, and A1P2 sensing films; (B) EDS spectrum from the A1P2 sensor.

X-ray photoelectron spectroscopy (XPS) analysis was carried out to clarify the chemical composition of the samples A1, P2 and A1P2, and the wide-scan spectra are shown in Fig. 4(A). All samples consisted of Sn, O, Pt and/or Ag. In Fig. 4(A) the Pt 4f peaks are visible, confirming the presence of platinum in the samples P2 and A1P2. Similarly, Ag 3d peaks are present which confirm the existence of silver in samples A1 and A1P2. The high-resolution spectrum in Fig. 4(B) shows that the main photoelectronic lines of Pt 4f are visible in the spectra of samples P2 and A1P2, but not in that of sample A1, as expected. Fig.4(B) shows two distinct peaks at 74.8 and 71.6 eV, respectively assigned to $4f_{5/2}$ and $4f_{7/2}$ signals from metallic Pt^0 [24]. The Pt 4f doublet in the spectrum of the Ag-Pt alloy sample (A1P2) is negatively shifted by 0.4 eV compared to that of the sample with pure Pt (P2) at 71.6 eV. The negative shift of the peaks

indicates a change from the Pt–Pt binding energy induced by the change in the electronic structure of Pt due to the interaction with Ag to form the alloy [25,26].

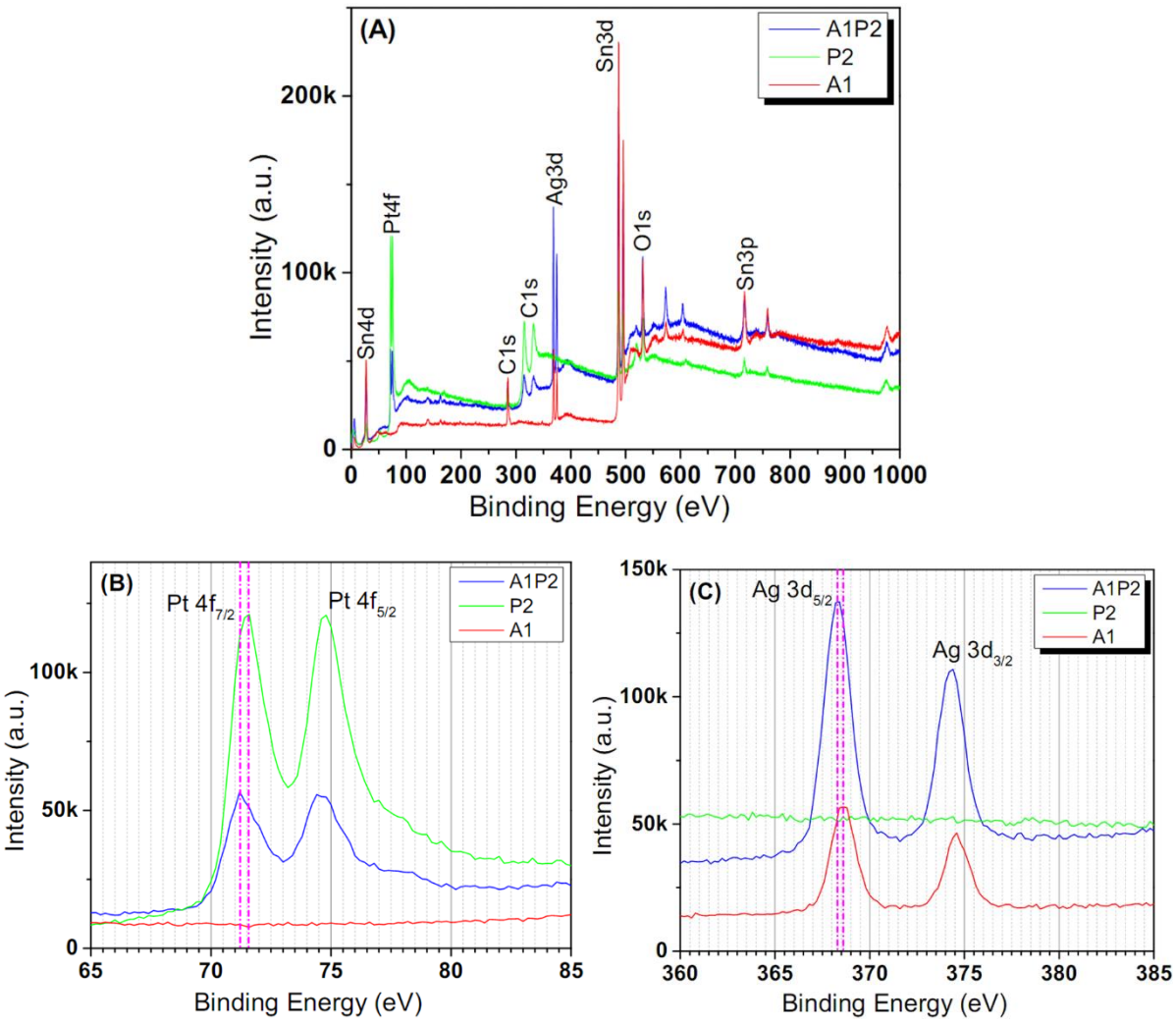

Figure 4. (A) XPS wide-scan spectra of the samples A1 (red), P2 (green) and A1P2 (blue); (B) high-resolution XPS spectra of Pt *4f* of samples A1, P2 and A1P2; (C) high-resolution XPS spectra of Ag *3d* of samples A1, P2 and A1P2.

The high-resolution spectra in Fig. 4(C) show that the main photoelectronic lines of Ag 3d are visible in samples A1 and A1P2, but not in that of sample P2, as expected. The figure shows two distinct peaks at 374.6 and 368.6 eV, assigned to the $3d_{3/2}$ and $3d_{5/2}$ signals of metallic Ag^0 [24]. The peaks in Fig. 4 (C) show a negative shift similar to that in Fig. 4 (B). The observed negative shift of the Ag 3d peaks is an indication of the charge transfer phenomena due to the formation of the Ag-Pt bimetallic nano-alloy, which leads to the change of the binding energy

from the metallic state of Ag [25,27]. According to [28], each peak is the convolution of two contributions corresponding respectively to Ag^0 and Ag^+ species.

The sensing response of the different thin films (pure SnO_2, SnO_2 decorated with Ag, with Pt and with Ag-Pt in different ratios) were studied as the dynamic resistance versus time. Each sensor was measured at four temperatures (200, 250, 300 and 350 °C) towards different concentrations of NH_3 (25, 50, 100 and 250 ppm), to compare their performance.

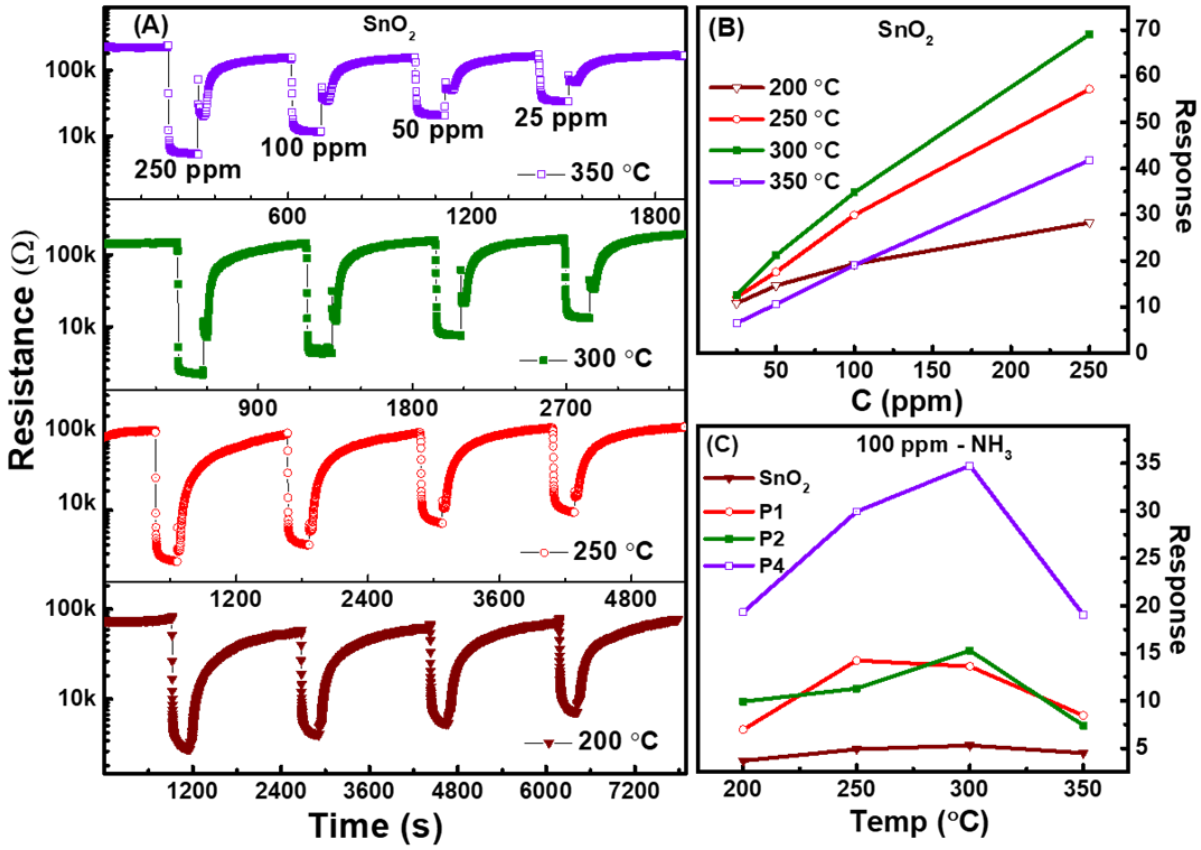

Figure 5. (A) Dynamic resistance of the pure SnO_2 sensor upon exposure to different concentrations of NH_3 at four temperatures; (B) Response of the sensor as a function of NH_3 concentration; (C) Response of the sensors decorated with Pt (P1, P2 and P4) and Ag (A1) to 100 ppm of NH_3, compared with that of the pure SnO_2 sensor, as a function of the working temperature.

Fig. 5(A) shows the dynamic resistance of the pure SnO_2 sensor at four temperatures. It is clear that the resistance suddenly drops as soon as NH_3 is injected into the measurement chamber and recovers its original value when the NH_3 flow is interrupted and an air flow is instead introduced into the chamber. This behavior is typical of *n*-type semiconductors when exposed

to reducing gas. It can also be seen from Fig. 5(A) that response time and recovery time decrease with increasing temperature. As the temperature increases from 200 to 350 °C, the average response time drops from 10.5 to 5.5 s, while the average recovery time drops from 1100 to 200 s. From the plots in Fig. 5(A), the sensor responses were calculated according to the definition given in the previous section for all NH_3 concentrations at the four temperatures and plotted in Fig. 5(B). At all temperatures the response increases with NH_3 concentration, as expected. The highest response values of 3.12, 3.77, 5.28 and 8.57 to 25, 50, 100 and 250 ppm of NH_3, respectively, were obtained at 300 °C.

Figure 5(C) shows the comparison between the responses towards 100 ppm of NH_3 of the sensors decorated with platinum (P1, P2 and P4), with silver (A1) and that of the pure SnO_2 sensor, as a function of temperature. The sensors decorated with Pt show much higher responses than the pure SnO_2 sensor, and the greater the amount of Pt, the greater the response to NH_3. As in the case of pure SnO_2, the maximum response occurs at 300 °C for all sensors, with the exception of sensor P1, for which it occurs at 250 °C. The maximum responses obtained are 5.28, 14.24, 15.29 and 34.78 respectively for the pure SnO_2, P1, P2 and P4 samples, demonstrating that surface decoration with Pt nanoparticles greatly improves the sensor performance.

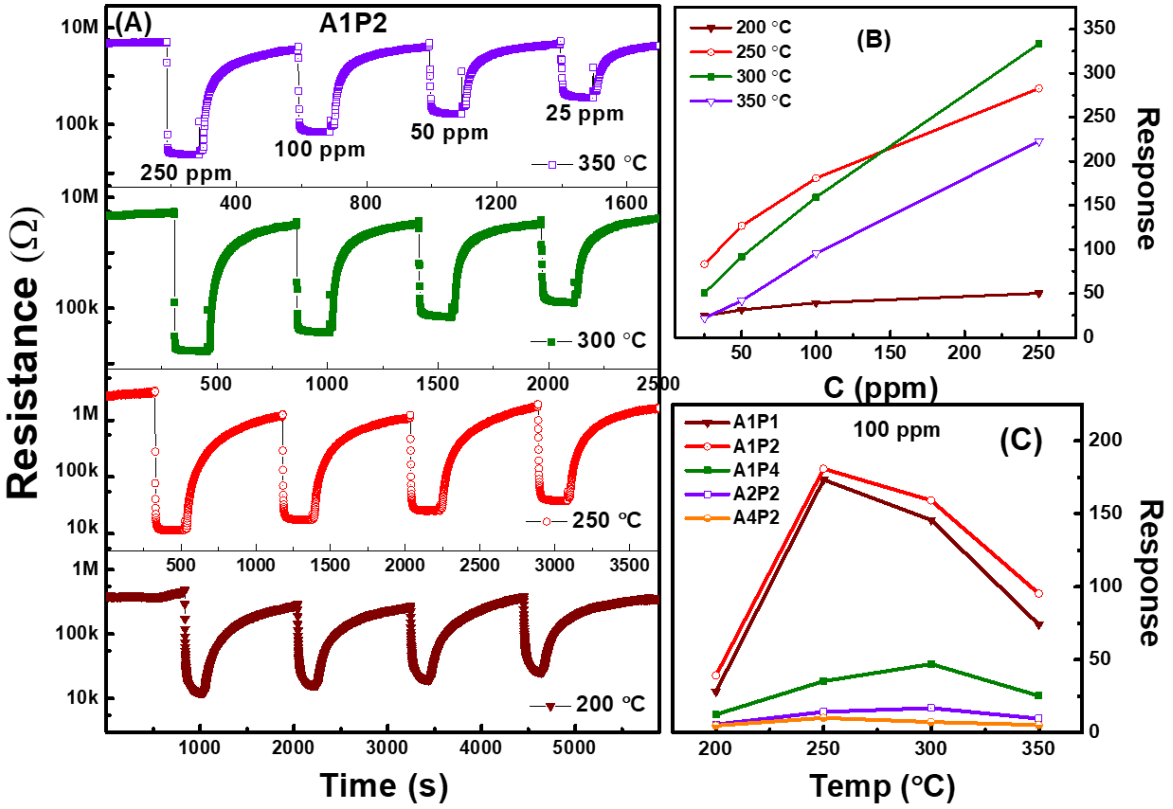

Figure 6. (A) Dynamic resistance of the A1P2 sensor upon exposure to different concentrations of NH_3 at various temperatures; (B) Calculated response of the A1P2 sensor; (C) Responses of all five Ag-Pt decorated sensors to 100 ppm of NH_3, as a function of the working temperature.

Since the sample decorated with 1 nm Ag (sample A1 in Table 1) also showed an improvement in sensor response towards NH_3 in Fig 5(C), the five sensors decorated with Ag-Pt alloy A1P1, A1P2, A1P4, A2P2 and A4P2 were investigated and compared. Figure 6(A) shows the dynamic resistance of sample A1P2, measured at different temperatures, at four different concentrations of NH_3. Comparing Fig. 6(A) with Fig. 5(A) it is clear that the resistance in air of the A1P2 sensor is much higher than that of the pure SnO_2 sensor, especially at high temperatures (5 MΩ instead of 220 kΩ at 350 °C). However, the behavior of the sensor is the same, namely the resistance undergoes a drastic drop when the sensor is exposed to NH_3 and returns to its original value when the sensor is exposed to dry air. Fig. 6(A) shows that the response time is only 12 s and the recovery time is 100 s at 250 °C, while the response time is 26 s and the recovery time is 560 s at 200 °C. Generally, the performance of the sensor improves with the increase of

temperature, but its performance at 250 °C is particularly interesting as is can be seen in Fig. 6(C). Figure 6(B) shows the sensor responses plotted as a function of the NH_3 concentration for different working temperatures. It is evident that the response increases almost linearly with the concentration of NH_3 at all temperatures. The response at low concentrations increases markedly as the temperature increases from 200 to 250 °C, and then decreases as the temperature increases. The response value of the A1P2 sensor at 250 °C increases from 78.84 to 263.78 as the NH_3 concentration increases from 25 to 250 ppm. At 300 °C, the response value raises from 43.46 to 325.53 at the same concentrations. Since the sensor is expected to operate at low NH_3 concentration (e.g. for breath analysis applications where NH_3 concentrations are approximately 1 ppm), the working temperature of 250 °C is chosen for further experiments. Figure 6(C) shows the response to 100 ppm of NH_3 of the sensors decorated with different amounts of Ag and Pt, as a function of the working temperature. It is clear that the A1P1 and A1P2 sensors achieve a far higher response at all temperatures than the other sensors, with the maximum value at 250 °C. At this temperature, the A1P1 sensor gives its maximum response of 173.4, while the A1P2 sensor gives an even higher response, of 180.9. Comparing the plots in Fig. 6(C), it is evident that the right amount of Ag and Pt used to decorate the surface of the SnO_2 thin film is very important for its sensing properties. These results agree with the studies by Peng [17] and Wisniewska [21] which showed that the Ag/Pt ratio affects the catalytic activity of the alloy. Since the A1P2 sample showed the best sensing performance, further experiments were carried out at lower NH_3 concentrations with this sensor at its optimal working temperature of 250 °C. The dynamic resistance of the A1P2 sensor in response to NH_3 concentrations from 0.25 to 5 ppm is shown in Fig. 7(A). It is evident that even at the concentrations below 1 ppm, the resistance drops drastically as soon as NH_3 is injected into the measurement chamber. The response values obtained for 0.25, 0.5, 1, 2.5 and 5 ppm are 1.50, 2.94, 4.31, 9.61 and 18.17, respectively. The limit of detection of the sensor towards NH_3 was calculated as 10 ppb. It should be noted that the calculation formula used here (see the end of

the Experimental section) produces an overestimated value of the limit of detection. This result demonstrates that the A1P2 sensor is suitable for use in early diagnostic applications through breath analysis, not only for its good and rapid response to NH_3, but also because of its low limit of detection towards this gas. However, breath analysis poses other challenges, such as moisture and other biomarkers present in the breath, which can interfere with the detection of the target NH_3 gas, as well as the stability of the sensor in such environment.

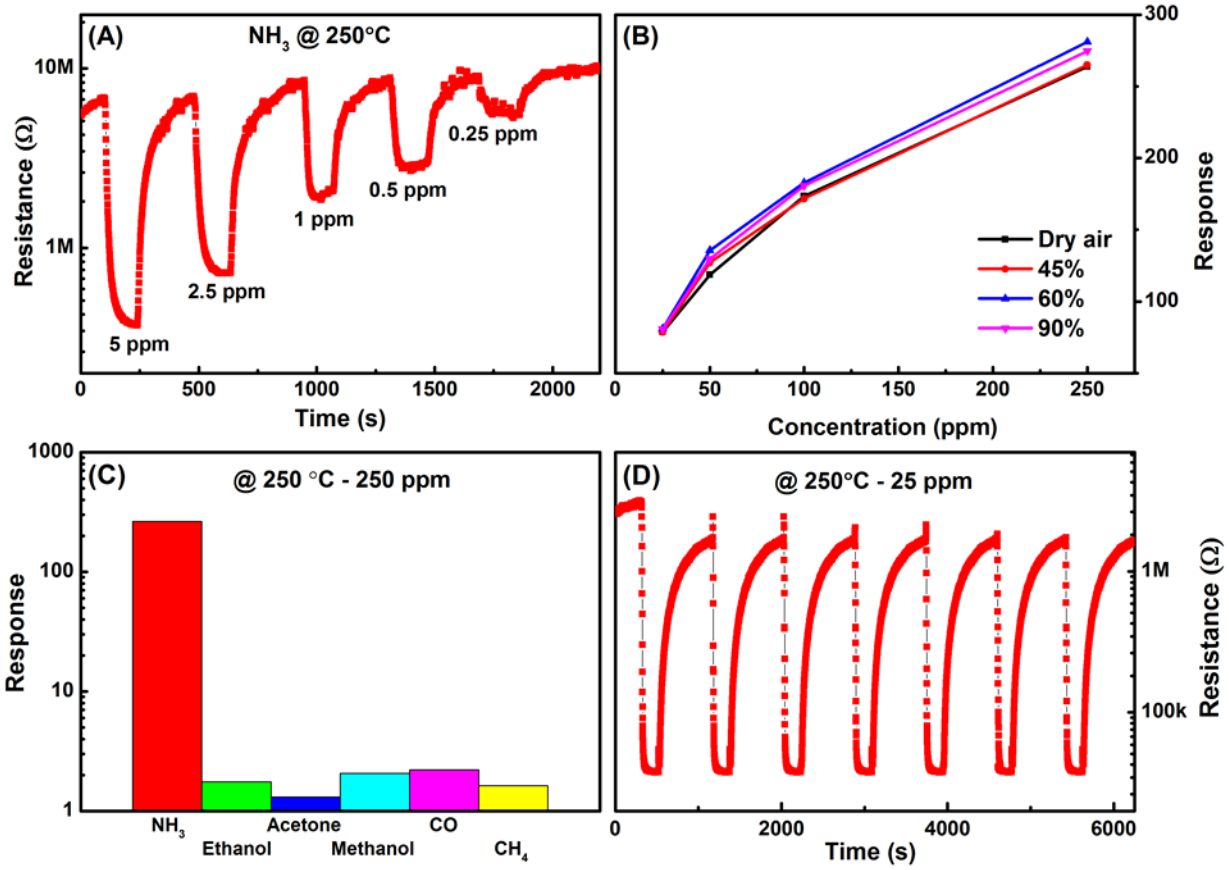

Figure 7. (A) Dynamic resistance of the A1P2 sensor at 250 °C to various concentrations of NH_3; (B) Sensor response to NH_3 in different humidity conditions; (C) Sensor selectivity at 250°C towards different gases; (D) Stability of the A1P2 sensor during seven response-recovery cycles to 25 ppm NH_3 at 250°C.

For this reason, the sensor was tested at the optimal temperature of 250 °C in various humidity conditions: dry air, 45%, 60%, and 90% RH. The results, shown in Fig. 7(B), demonstrate that

the sensor response changes negligibly under very different humidity conditions, especially at the lower concentrations of NH_3. Furthermore, the selectivity of the A1P2 sensor was tested at 250 °C towards 250 ppm of NH_3, ethanol, acetone, methanol, CO and CH_4 (as possible interfering gases in human breath), as shown in Fig. 7(C). The sensor shows excellent selectivity (the logarithmic scale for the Y axis should be noted) with response values of 263.78, 1.75, 1.31, 2.07, 2.21 and 1.63 for NH_3, ethanol, acetone, methanol, CO and CH_4, respectively. Considering the definition of selectivity as the ratio between the response to the target gas and the response to the most difficult interferer, a value of about 120 is obtained. Finally, the stability of the sensor was tested by measuring seven response-recovery cycles to 25 ppm of NH_3 at the working temperature of 250 °C. The results in Fig. 7(D) show that the sensor response is fast and stable.

As can be seen in Fig. 4(C), the response of the samples A1 and P2 to 100 ppm NH_3 at 250 °C are 4 and 11, respectively, whereas the response of the sample A1P2 in Fig. 5(C) under the same conditions is 176. Notably, the sample A1P2 decorated with the bimetal catalyst has the same amount of Ag and Pt as the two samples A1 and P2 with single catalysts. Therefore, the sensing mechanism underlying the huge improvement of the sensor performance might be attributed to the increased catalyst properties of the Ag-Pt bimetallic nanoalloy particles compared to those of the single metallic Ag or Pt particles with which the other samples are decorated.

It is believed that the amount of Ag equivalent to 1 nm layer cannot form a continuous Ag layer, but clusters of a few Ag atoms on the rather rough surface of SnO_2, as shown in Fig. 2. The dispersed Ag NPs react with Pt when in contact, especially during the heat treatment at 500 °C for 3 hours. The diffusion of Ag into Pt changes their chemical state, as a large number of Ag atoms are included in the alloy. Since the electronegativity of Pt is higher than that of Ag (2.29 vs. 1.92), it is reasonable to assume that the amount of Pt is large enough to consume as much Ag as possible to form the alloy, without covering the whole surface of the underlying SnO_2

material. This is clearly manifested in Fig. 6(C), where the optimal ratio between Ag and Pt is 1 to 2 nm. The ratio between the two materials is therefore important as they form alloy, because it tunes the catalytic effect of the nanoparticles [21], improving the sensor performance. In our previous publication [29], the SnO_2 film decorated with a 5 nm layer of Pt showed the highest response of 46.3 to 100 ppm NH_3 at the working temperature of 250 °C. It is clear that the catalytic effect of the Ag-Pt nanoalloy significantly improved the sensing properties to NH_3 compared to the single metals.

The superior catalytic effect of the bimetallic NPs [30] can be explained by two different mechanisms. On one hand, the metallic nanoparticles on the SnO_2 surface are more reactive than the metal oxide and help to dissociate the impinging gas molecules. In this way, when the sensor is in air, the presence of bimetallic catalytic NPs helps the transformation of neutral oxygen molecules into O^- ions with high chemical activity. This results in a higher density of oxygen adsorbed on the surface of the thin film, and therefore a more intense depletion of the charge carriers from its lattice (Fig. 9, in air), causing an increase in the sensor resistance. The NH_3 molecules hitting the surface of the Ag-Pt-decorated SnO_2 sensor interact with the adsorbed oxygen according to Equation (3.1), releasing electrons:

$$2NH_3 + 3O^-_{(ADS)} \rightarrow N_2 + 3H_2O + 3e^- \quad (1)$$

$$2NH_3 \rightarrow 2NH_2 + H_2 \quad (2)$$

The electrons released in the reaction return to the nanostructured thin film and participate again in conduction, thus lowering the resistance of the sensor (Fig. 9, in NH_3 environment). Since the sensor response is defined as the ratio between its resistance in air and its resistance in NH_3 environment, the high initial resistance in air due to the presence of catalytic nanoparticles can greatly increase its value.

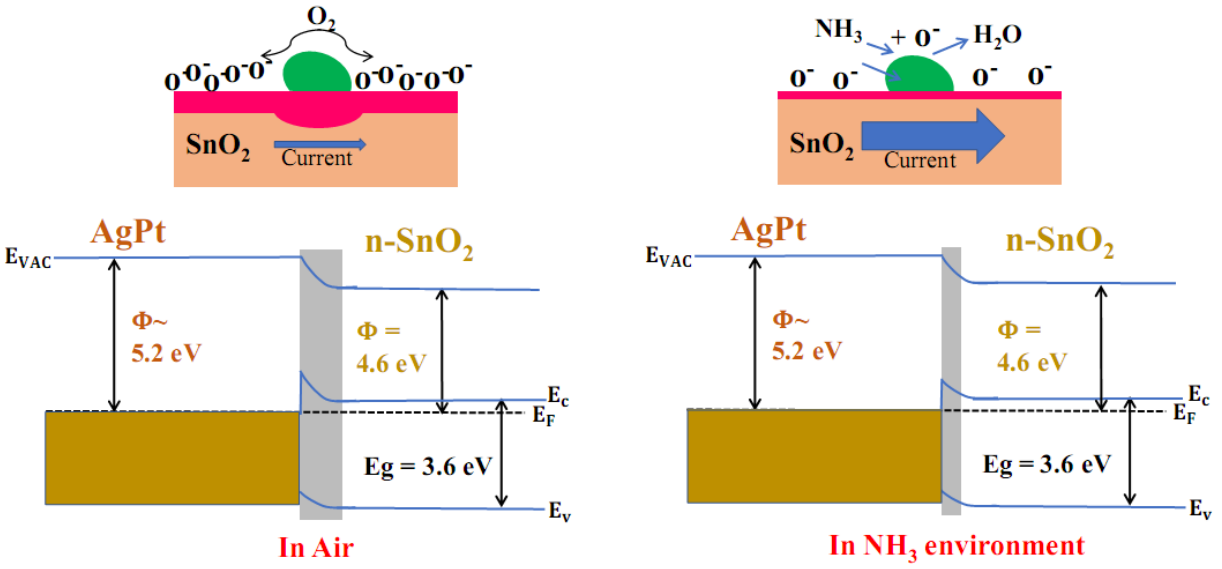

Figure 9. The mechanism of gas sensing of the SnO_2 sensor modified by Ag/Pt.

On the other hand, a Schottky barrier is formed at the interface between the metallic nanoparticle and the metal oxide semiconductor. This happens because the work function of Ag-Pt alloy is Φ_{AgPt} = 5.2 eV [31], while that of SnO_2 is Φ_{SnO_2} = 4.6 eV [32]. The equalization of the Fermi level in the two materials creates a potential barrier that is proportional to the difference between the metal-vacuum work function and the semiconductor-vacuum electron affinity. As can be seen in Fig. 9, the band bending due to the metal-semiconductor interface attracts the electrons from SnO_2 to the Ag-Pt alloy creating a depletion layer in the SnO_2. This depletion zone reduces the number of electrons that can participate in conduction similarly to that on the surface of the thin film (due to oxygen adsorption) and therefore greatly increases the sensor resistance: 5 MΩ instead of 220 kΩ, as can be seen by comparing the plots at 350 °C in Fig. 6(A) and 5(A). When the NH_3 molecules come into contact with the sensor, they react with the adsorbed oxygen according to Eq. (1), or they dissociate as a result of the catalytic bimetal NPs, according to Eq. (2). The atomic hydrogen then diffuses into the metal catalyst forming intermediate compounds and thus reducing the Schottky barrier at the interface between the metal and the semiconductor. This reduces the depletion zone, thereby releasing electrons and greatly reducing the sensor resistance. The improved response of the decorated

sensor comes mainly from the initial condition of the nanostructured thin film, which is much more deeply depleted of electrons than that of the pure SnO_2 thin film. When the NH_3 molecules and their radicals react with the absorbed oxygen releasing electrons, the conductivity of the material increases strongly, leading to an ultra-high response. A higher response is especially important because it leads to a lower limit of detection.

Conclusions

In an attempt to develop an NH_3 gas sensor for breath analysis, different gas sensors based on pure SnO_2 thin films and on SnO_2 thin films decorated with Ag, Pt and Ag-Pt NPs were fabricated and tested against different concentrations of NH_3 at different temperatures. It was found that decoration with the metallic NPs as catalysts always improved the performance of the sensors, and that the nanoalloy of Ag and Pt led to the best results. Furthermore, the amount of Ag and Pt could be adjusted to obtain the optimal response. The best performance were obtained with the SnO_2 sensor decorated with both Ag (1 nm) and Pt (2 nm) working at 250 °C. At 250 °C the sensor responded strongly to 1 ppm NH_3 (response of 4.31) and quickly (response time of 12 s) showing a very low detection limit of 10 ppb. The sensor response was stable and negligibly affected by humidity in a wide range (0 - 90% RH) or by interfering gases such as ethanol, acetone, methanol, CO and CH_4 (selectivity of 120). The results demonstrated that the SnO_2 sensor decorated with both Ag and Pt, equivalent to sputtered layers of 1 and 2 nm respectively, is an ideal candidate for breath analysis applications.

Conflict of Interest

The authors have no conflict of interest to declare.

Acknowledgements

XXXXX

References

[1] B. Timmer, W. Olthuis, A. Van Den Berg, Ammonia sensors and their applications - A review, Sensors Actuators, B Chem. 107 (2005) 666–677. doi:10.1016/j.snb.2004.11.054.

[2] R. Chanonsirivorakul, N. Nimsuk, Analysis of Relationship between the Response of Ammonia Gas Sensor and Odor Perception in Human, in: 2020 8th Int. Electr. Eng. Congr., IEEE, 2020: pp. 1–4. doi:10.1109/iEECON48109.2020.229522.

[3] L.G. Close, F.I. Catlin, A.M. Cohn, Acute and Chronic Effects of Ammonia Burns of the Respiratory Tract, Arch. Otolaryngol. - Head Neck Surg. 106 (1980) 151–158. doi:10.1001/archotol.1980.00790270015004.

[4] S.S. Mohiuddin, D. Khattar, Biochemistry, Ammonia, StatPearls Publishing, Treasure Island (FL), 15 May 2019. ID: NBK541039PMID: 31082083, (n.d.).

[5] L.R. Narasimhan, W. Goodman, C.K.N. Patel, Correlation of breath ammonia with blood urea nitrogen and creatinine during hemodialysis, Proc. Natl. Acad. Sci. 98 (2001) 4617–4621. doi:10.1073/pnas.071057598.

[6] D.J. Kearney, T. Hubbard, D. Putnam, Breath ammonia measurement in Helicobacter pylori infection, Dig. Dis. Sci. 47 (2002) 2523–2530. doi:10.1023/A:1020568227868.

[7] S. Yi, S. Tian, D. Zeng, K. Xu, X. Peng, H. Wang, S. Zhang, C. Xie, A novel approach to fabricate metal oxide nanowire-like networks based coplanar gas sensors array for enhanced selectivity, Sensors Actuators B Chem. 204 (2014) 351–359. doi:10.1016/j.snb.2014.07.076.

[8] W. Guo, X. Duan, Y. Shen, K. Qi, C. Wei, W. Zheng, Ionothermal synthesis of mesoporous SnO_2 nanomaterials and their gas sensitivity depending on the reducing ability of toxic gases, Phys. Chem. Chem. Phys. 15 (2013) 11221. doi:10.1039/c3cp51663f.

[9] M. Shahabuddin, A. Umar, M. Tomar, V. Gupta, Custom designed metal anchored SnO_2 sensor for H_2 detection, Int. J. Hydrogen Energy. 42 (2017) 4597–4609. doi:10.1016/j.ijhydene.2016.12.054.

[10] N.S. Ramgir, Y.K. Hwang, S.H. Jhung, H.-K. Kim, J.-S. Hwang, I.S. Mulla, J.-S. Chang, CO sensor derived from mesostructured Au-doped SnO_2 thin film, Appl. Surf. Sci. 252 (2006) 4298–4305. doi:10.1016/j.apsusc.2005.07.015.

[11] N. Yamazoe, Y. Kurokawa, T. Seiyama, Effects of additives on semiconductor gas sensors, Sensors and Actuators. 4 (1983) 283–289. doi:10.1016/0250-6874(83)85034-3.

[12] S.-W. Choi, A. Katoch, G.-J. Sun, S.S. Kim, Bimetallic Pd/Pt nanoparticle-functionalized SnO_2 nanowires for fast response and recovery to NO_2, Sensors Actuators B Chem. 181 (2013) 446–453. doi:10.1016/j.snb.2013.02.007.

[13] N.X. Thai, N. Van Duy, N. Van Toan, C.M. Hung, N. Van Hieu, N.D. Hoa, Effective monitoring and classification of hydrogen and ammonia gases with a bilayer Pt/SnO_2 thin film sensor, Int. J. Hydrogen Energy. 45 (2020) 2418–2428. doi:10.1016/j.ijhydene.2019.11.072.

[14] D. Degler, S.A. Müller, D.E. Doronkin, D. Wang, J.-D. Grunwaldt, U. Weimar, N. Barsan, Platinum loaded tin dioxide: a model system for unravelling the interplay

between heterogeneous catalysis and gas sensing, J. Mater. Chem. A. 6 (2018) 2034–2046. doi:10.1039/C7TA08781K.

[15] Y.-D. Wang, X.-H. Wu, Q. Su, Y.-F. Li, Z.-L. Zhou, Ammonia-sensing characteristics of Pt and SiO_2 doped SnO_2 materials, Solid. State. Electron. 45 (2001) 347–350. doi:10.1016/S0038-1101(00)00231-8.

[16] M. Shahabuddin, A. Sharma, J. Kumar, M. Tomar, A. Umar, V. Gupta, Metal clusters activated SnO_2 thin film for low level detection of NH_3 gas, Sensors Actuators B Chem. 194 (2014) 410–418. doi:10.1016/j.snb.2013.12.097.

[17] Z. Peng, H. You, H. Yang, An electrochemical approach to PtAg alloy nanostructures rich in Pt at the surface, Adv. Funct. Mater. 20 (2010) 3734–3741. doi:10.1002/adfm.201001194.

[18] I.-S. Hwang, J.-K. Choi, H.-S. Woo, S.-J. Kim, S.-Y. Jung, T.-Y. Seong, I.-D. Kim, J.-H. Lee, Facile Control of C_2H_5OH Sensing Characteristics by Decorating Discrete Ag Nanoclusters on SnO_2 Nanowire Networks, ACS Appl. Mater. Interfaces. 3 (2011) 3140–3145. doi:10.1021/am200647f.

[19] W. He, X. Wu, J. Liu, K. Zhang, W. Chu, L. Feng, X. Hu, W. Zhou, S. Xie, Pt-Guided Formation of Pt-Ag Alloy Nanoislands on Au Nanorods and Improved Methanol Electro-Oxidation, Am. Chem. Soc. 1113 (2009) 10505–10510.

[20] A.A. Umar, E. Rahmi, A. Balouch, M.Y.A. Rahman, M.M. Salleh, M. Oyama, Highly-reactive AgPt nanofern composed of {001}-faceted nanopyramidal spikes for enhanced heterogeneous photocatalysis application, J. Mater. Chem. A. 2 (2014) 17655–17665. doi:10.1039/c4ta03518f.

[21] J. Wisniewska, M. Ziolek, Formation of Pt–Ag alloy on different silicas – surface properties and catalytic activity in oxidation of methanol, RSC Adv. 7 (2017) 9534–9544. doi:10.1039/C6RA28365A.

[22] J. Kaur, S.C. Roy, M.C. Bhatnagar, Highly sensitive SnO_2 thin film NO_2 gas sensor operating at low temperature, Sensors Actuators B Chem. 123 (2007) 1090–1095. doi:10.1016/j.snb.2006.11.031.

[23] H.-J. Qiu, H.T. Xu, X. Li, J.Q. Wang, Y. Wang, Core–shell-structured nanoporous PtCu with high Cu content and enhanced catalytic performance, J. Mater. Chem. A. 3 (2015) 7939–7944. doi:10.1039/C5TA00020C.

[24] J.-J. Feng, X.-X. Lin, L.-X. Chen, M.-T. Liu, J. Yuan, A.-J. Wang, Ionic liquid-assisted synthesis of composition-tunable cross-linked AgPt aerogels with enhanced electrocatalysis, J. Colloid Interface Sci. 498 (2017) 22–30. doi:10.1016/j.jcis.2017.03.042.

[25] E. Fidiani, G. Thirunavukkarasu, Y. Li, Y.-L. Chiu, S. Du, Ultrathin AgPt alloy nanorods as low-cost oxygen reduction reaction electrocatalysts in proton exchange membrane fuel cells, J. Mater. Chem. A. 8 (2020) 11874–11883. doi:10.1039/D0TA02748K.

[26] H. Liu, F. Ye, Q. Yao, H. Cao, J. Xie, J.Y. Lee, J. Yang, Stellated Ag-Pt bimetallic nanoparticles: An effective platform for catalytic activity tuning, Sci. Rep. 4 (2015) 3969. doi:10.1038/srep03969.

[27] C. Fang, J. Zhao, G. Zhao, L. Kuai, B. Geng, Simultaneous tunable structure and composition of PtAg alloyed nanocrystals as superior catalysts, Nanoscale. 8 (2016) 14971–14978. doi:10.1039/C6NR02643E.

[28] Y. Yang, W. Wang, Y. Liu, F. Wang, Z. Zhang, Z. Lei, Carbon supported heterostructured Pd–Ag nanoparticle: Highly active electrocatalyst for ethylene glycol oxidation, Int. J. Hydrogen Energy. 40 (2015) 2225–2230. doi:10.1016/j.ijhydene.2014.12.054.

[29] N. Van Toan, C. Manh, N. Duc, N. Van Duy, Enhanced NH3 and H2 gas sensing with H2S gas interference using multilayer SnO_2/Pt/WO_3 nanofilms, 412 (2021).

[30] W. He, X. Wu, J. Liu, X. Hu, K. Zhang, S. Hou, W. Zhou, S. Xie, Design of AgM bimetallic alloy nanostructures (M = Au, Pd, Pt) with tunable morphology and peroxidase-like activity, Chem. Mater. 22 (2010) 2988–2994. doi:10.1021/cm100393v.

[31] S.Y. Lim, K. Ha, H. Ha, S.Y. Lee, M.S. Jang, M. Choi, T.D. Chung, Three-dimensionally patterned Ag–Pt alloy catalyst on planar Si photocathodes for photoelectrochemical H_2 evolution, Phys. Chem. Chem. Phys. 21 (2019) 4184–4192. doi:10.1039/C8CP07304J.

[32] T.T. Ngoc Hoa, N. Van Duy, C.M. Hung, N. Van Hieu, H.H. Hau, N.D. Hoa, Dip-coating decoration of Ag_2O nanoparticles on SnO_2 nanowires for high-performance H_2S gas sensors, RSC Adv. 10 (2020) 17713–17723. doi:10.1039/D0RA02266G.